

Controlling a mechanical oscillator with a tunable coherent feedback network

Joseph Kerckhoff,^{1,*} Reed W. Andrews,¹ H. S. Ku,¹ William F. Kindel,¹
Katarina Cicak,² Raymond W. Simmonds,² and K. W. Lehnert¹

¹*JILA, National Institute of Standards and Technology and the University of Colorado, Boulder, Colorado 80309, USA*

²*National Institute of Standards and Technology, Boulder, CO 80305, USA*

(Dated: December 3, 2024)

We demonstrate a fully cryogenic microwave feedback network composed of modular superconducting devices interconnected by transmission lines and designed to control a mechanical oscillator coupled to one of the devices. The network is partitioned into an electromechanical device and a dynamically tunable controller that coherently receives, processes and feeds back continuous microwave signals that modify the dynamics and readout of the mechanical state. While previous electromechanical systems represent some compromise between efficient control and efficient readout of the mechanical state, as set by the electromagnetic decay rate, this flexible controller yields a closed-loop network that can be dynamically and continuously tuned between both extremes much faster than the mechanical response time. We demonstrate that the microwave decay rate may be modulated by at least a factor of 10 at a rate greater than 10^4 times the mechanical response rate.

INTRODUCTION

Feedback methodologies underlie or are a key to understanding robust systems in all fields of science and technology. Analyzing complex natural systems (e.g. biological processes, financial markets, Earth’s climate) and engineered systems (e.g. electrical circuits, autonomous vehicles, utility grids) in terms of real-time feedback illuminates their dynamics. Moreover, the proper application of feedback is an essential ingredient in the successes of James Watt, the Wright brothers, automated industrial production, scanning tunneling microscopes, and a decentralized internet, to name a few [1]. As researchers rapidly improve their ability to engineer fully coherent electromagnetic (EM) devices that operate at the quantum level, we should start to look beyond individual components to find experimental and theoretical techniques that exploit *coherent networks* of quantum devices. In particular, given the extreme demands of quantum-scale engineering one must anticipate that engineered feedback will be essential in realizing useful complex systems [2–4]. Models that adapt concepts from control systems engineering handle the complexity of such networks much better than approaches entirely native to the Physics community [5, 6]. However, despite some progress [4–16], a systematic craft of control design using coherent systems is lacking. Coherent EM control design is more restrictive than traditional electrical circuit design since the technologies used must be describable by unitary processes [5, 7–9]. As such, fully coherent EM control systems designed to tune even classical dynamical processes [11, 13] can help advance researchers towards the goal of a systematic craft of quantum control.

In general, the uses of feedback are two-fold: feedback is employed to tune the dynamics of an otherwise untunable system, and/or to enhance a system’s robustness [1]. In the past decade, electromechanical technologies, in which mechanical simple harmonic oscillators (hereon

“oscillators”) are coupled to itinerant EM fields, have become increasingly coherent and powerful (such systems are also called “optomechanical”), e.g. [17–21]. Oscillators are more isolated from thermal baths and their interactions with distinct EM modes are better controlled. As a consequence, these devices are often module-like and unadjustable. Prioritizing a monolithic and insular design, important characteristics like EM center frequency and linewidth are often fixed by construction, and often a single EM input/output (I/O) port admits experimental access to all internal mechanisms in high performance devices [19, 21]. In principle, tunability may be won back without compromising device integrity by employing a coherent controller that exchanges continuous coherent signals with this port. Here, we demonstrate a coherent feedback network of coherent EM devices, a coherent superconducting electromechanical device [18, 19, 22–27] and a coherent superconducting microwave controller [13, 28], that provides a previously unavailable degree of dynamic flexibility in how an electromechanical oscillator may be controlled and measured. While our network is too complex for traditional electromechanical models [17, 29, 30], it requires only three components, all of which are accessible to superconducting circuit labs (and feature regularly in our own work [19, 20, 31]), and is efficiently and intuitively modeled as a linear feedback system [1, 5, 9]. In other words, this network is easy to build (given current device technologies) and its mechanisms easy to intuit. But it is difficult to model quantitatively, meriting methods that naturally handle complex networks. Because this perspective is relatively novel in electromechanics [10, 32, 33], this article features a pedagogical modeling section that outlines the network modeling method and its advantages (rigorous derivations are well-covered in the literature, e.g. [5, 6, 9, 10]). Also, because it employs theoretical approaches developed by an electrical engineering community, familiar concepts in electromechanics are described in more detail than usual.

The coherent control approach is roughly analogous to using Watt’s centrifugal governor to regulate a steam engine, in that the controller and the system to be controlled (the “plant”) are built using similar technologies and the dual processes of sensing and actuation are effectively inseparable [11–13]. Such an approach is distinct from measurement-based approaches, in which coherent signals produced by the plant are measured, the measurements are interpreted by an incoherent controller (often a computer), and the controller synthesizes new signals that act back on the plant [34–40]. In comparison, coherent control systems are more physically compact. They also make better use of given resources — e.g., a coherent controller has access to both quadratures of a coherent signal, without any added noise [8, 10].

This network was inspired by a new, coherent feedback interpretation of the common electromechanical technique of “sideband cooling” [17, 19, 21, 22, 25, 41–44], described in the next paragraph. While previous electromechanical systems make some compromise between better mechanical control and better mechanical measurement capabilities, we demonstrate that this network may be dynamically modulated between both extremes. This is equivalent to alternately isolating the oscillator from and coupling it to fields outside the network, without modifying its coupling to intra-network fields, a critical capability in many quantum engineering proposals. Such capabilities have featured in the superconducting qubit community, for example, using custom-made devices [45, 46], but our approach differs even from these in that tunability is achieved through an unconventional network of relatively conventional devices. As for applications in electromechanics, this network allows for mechanical states to be alternately manipulated efficiently and read out efficiently. Or the waveform of signals entering or exiting the network could be modulated, facilitating electromechanical state transfer in future work [20, 47]. This network is also equivalent to a different, proposed network that outperforms traditional methods of stabilizing an electromechanical oscillator [10].

THE NETWORK AND PHYSICAL INTUITION

Sideband cooling is a widely used electromechanical technique [17, 19, 21, 22, 25, 41–44]. The canonical sideband cooling system consists of an EM resonator coupled to a mechanical oscillator and driven at a frequency below the EM resonance. Mechanical cooling via this method is usually explained in analogy to early ion trapping experiments [17, 29, 30, 48]. A small portion of the low-entropy EM drive is inelastically scattered by the mechanical oscillator in the resonator, with each scattered photon having gained or lost a phonon’s worth of energy. If the center frequency of the resonator is higher than the drive frequency, then more frequency up-converted pho-

tons are scattered than down-converted photons. Consequently, the oscillator gives up energy on average to the EM field per scattering event, reducing its motion. This phenomenon is usually visible through “blue” (up-converted) and “red” (down-converted) sidebands to the “coupling tone” (drive carrier) emitted by the resonator. A cooling oscillator is indicated by more blue than red sideband power, less total sideband power, and sideband power spectral densities broader than the intrinsic oscillator linewidth.

There are also coherent feedback interpretations of the same system [10, 32, 33], but they are seldom emphasized. For instance, one may view the input coupler to the resonator as a controller that receives a continuous stream of information about the mechanical motion and synthesizes a reactive feedback signal counteracting this motion. If the resonator is a single-sided Fabry-Perot cavity and the oscillator is the spring-mounted mass of the perfectly reflecting mirror [17, 36, 42, 43], for example, the partially-transmissive input mirror acts as a coherent controller. As the mirror mass moves forward or backward, optical signals reflecting off it are Doppler shifted and arrive at the input mirror with a positive or negative phase shift, respectively. The input mirror is designed such that, through interference with an external drive, more or less light is coupled into the cavity when the phase shift is positive or negative, respectively. Higher intracavity power counteracts forward motion of the mass through radiation pressure, while lower intracavity power encourages a retreating mass to be pushed forward by its spring. Thus the mass feels a light-induced drag, reducing its motion. The analogous, measurement-based control approach would have no input mirror, but the phase of light reflecting off the mass would be measured and used to apply a counteracting force to the oscillator [8, 10, 36]. To our knowledge, it is novel to identify the input coupler as the controller, but with this perspective it is clear that employing a single, partially transmissive mirror is but one control design. Instead, the controller could be an entire coherent subsystem [8, 10], offering different types of control over the oscillator. For example, placing another, non-absorptive optical filter (e.g. another cavity) between the external drive and input mirror adds additional optical feedback paths, modifying the optical forces felt by the oscillator. For non-ideal (i.e. partially absorptive) or complex (i.e. multi-mode) coherent control networks, though, techniques borrowed from network systems theory [9] are vital for tractable modeling of the entire system

The choice of an input coupler in an electromechanical system typically represents a compromise. For example, resonators with weak couplers effectively “integrate” Doppler-shifted signals for longer, and can consequently respond to finer mechanical motion [19, 21] (is efficient at “control”). However, weak couplers frustrate high-

bandwidth detection of mechanical motion by low-pass filtering mechanical information on EM signals leaving the system and encouraging loss of the same through parasitic channels (is less suited for “measurement”). Conversely, relatively strong couplers produce systems that favor mechanical measurement over control [31, 36]. A “weak” (“strong”) coupler is one that produces a resonator linewidth κ_t narrower (broader) than the center frequency of the oscillator Ω , yielding what is known as a “resolved-sideband” (“unresolved-sideband”) system. In both choices, the coupler-controller is both passive and (in all electromechanical systems to our knowledge) fixed at the time of construction. Here, we take an alternate approach and control the oscillator with a dynamically tunable coherent subsystem, enabling a wider range of control and measurement capabilities.

Generically, many superconducting microwave realizations of electromechanical systems consist of a high quality microwave LC resonator, in which the capacitance is modulated by a spring-loaded mass [19, 22, 24–27, 31]. Motion in this mechanical oscillator adjusts the capacitance of the resonator, and thus acts on microwave photons in the resonator. And the voltage potential across the capacitor creates a Coulomb force that acts on the oscillator, and thus the number of microwave photons in the resonator acts on the position of the oscillator. Via an inductive transformer, the intrinsically low-loss resonator couples weakly to a 50Ω transmission line, which serves as the I/O port through which the electromechanical device is probed, driven and controlled. This input transformer, through which microwave fields internal and external to the resonator interfere, traditionally serves the same role as the input mirror in the Fabry-Perot system described above. This microwave system is accurately described at a quantum level with a model that is formally equivalent to the models used to describe electromechanical systems of all scales and realizations [22, 29, 30, 44]. Although the specific electromechanical circuit (EMC) used here is somewhat incidental, it is a new design of this type [27], built from a 4.672 GHz center frequency and over-coupled $\kappa_t/2\pi = 2.8$ MHz resonator, employing an oscillator with an effective mass of ~ 10 ng, center frequency of $\Omega = 2\pi \times 713.6$ kHz and intrinsic linewidth of $\Gamma_0 = 2\pi \times 0.81$ Hz, and in which each photon exerts a force on the oscillator (in coherent amplitude units) of $g_0 = \hbar \times 2.3$ Hz.

Many superconducting microwave electromechanical experiments conducted by us [19, 20, 22, 31] and others [23–25, 44] are partitioned into an “upstream” electromechanical circuit (EMC), containing an oscillator to be studied, and a “downstream” cryogenic low- or near quantum limited-noise temperature amplifier, for high-fidelity readout of microwave probes. Our group typically uses near quantum-limited Josephson parametric amplifiers (JPAs) for readout [28]. JPAs are composed of a 20dB directional coupler followed by a single-port

“tunable Kerr circuit” (TKC) [13, 28], a nonlinear microwave resonator whose center frequency is drive power-dependent and tunable with an applied magnetic flux.

Housed in a dilution refrigerator, our network is the interconnection of a single-port EMC, a JPA, and a microwave tee (Fig. 1a). The EMC and JPA are connected to one tee port each, while the remaining tee port serves as the overall I/O network port. The network output is amplified by a cryogenic HEMT for analysis. While the EMC and TKC were originally intended for different experiments and were mounted in separate sample boxes, and interconnections were made using \sim cm-length coplanar waveguides and low-loss, semi-rigid coaxial cables, an analogous network could be fabricated on a single Si substrate. In this report, we do not pump our JPA; effectively, it is operated as a gain-1 amplifier, or more precisely, as a linear resonator whose center frequency can be tuned by applying either magnetic flux or a moderate amount of microwave drive power. We do, however, typically employ a cancellation tone that prevents the carrier of any strong, electromechanical coupling tone driving the network from reaching the TKC and driving

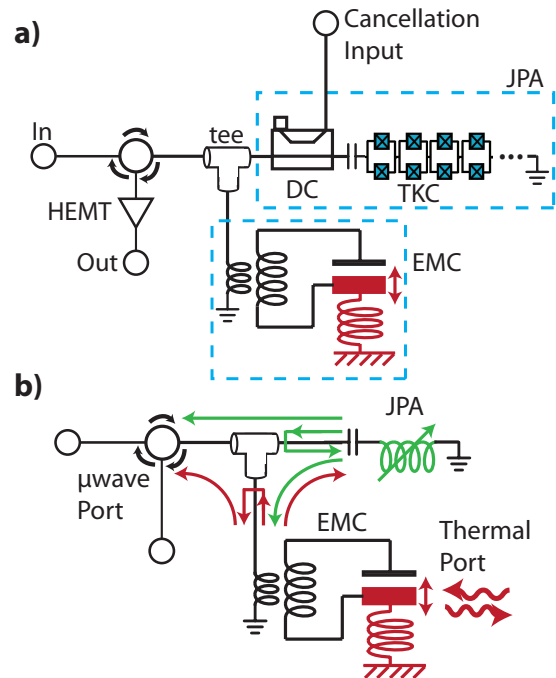


FIG. 1: a) An experimental schematic of the coherent feedback network. A microwave tee connects an electromechanical circuit (EMC) to a Josephson parametric amplifier (JPA) — here broken down into its directional coupler (DC) and tunable Kerr circuit (TKC) subcomponents — and provides an overall input-output port. The In port is typically driven by a strong electromechanical coupling tone, but this tone is typically cancelled at the DC, preventing its strong carrier from driving the TKC nonlinear. Microwave signals are detected at the Out port. b) Conceptual schematic of coherent interconnections. Ideally, the JPA acts as an over-coupled and wide-band linear resonator with a tunable center frequency.

it nonlinear.

Conceptually, the network’s operation is depicted in Fig. 1b. Microwave signals leaving the EMC and carrying information about the motion of the oscillator are split three ways at the tee: most of the amplitude is split evenly between the network output and the JPA input, and a small amount is reflected. Modeling the JPA as a linear resonator with a tunable center frequency, the JPA reflects its signal portion with a tunable phase shift. Similarly split by the tee, a portion of the JPA-reflected signal interferes with the EMC-to-output signal, enhancing or diminishing the rate of mechanical information leaving the network. The portion of the JPA-reflected signal fed back to the EMC can exert a force on the mechanical oscillator, amplifying or counteracting its motion. Both effects are controlled by a single, continuous parameter — the JPA center frequency — and both effects improve as the JPA bandwidth exceeds the bandwidth of the EMC and the EMC bandwidth exceeds the oscillator’s center frequency. This network may be interpreted as analogous to the Fabry-Perot optomechanical system, except with a user-controlled knob that simultaneously modifies the reflectivity and position of the input mirror [46]. This network may also be interpreted as a feedback control system: rather than make a room-temperature measurement of the JPA output, this signal is fed back directly to the EMC without leaving the cryostat. In this work, the former interpretation aids physical intuition, but the later is required in quantitative considerations. Ideally, the JPA’s transformation of the microwave signal is unitary (i.e. adds no noise), and this feedback network is fully coherent and thus fundamentally different from any measurement-based control system [5, 7–10].

MODEL

Each subcomponent is separably described by an I/O dynamical model, a familiar concept in quantum optics [5, 49] and superconducting microwave systems [13, 50]. Moreover, despite fundamental nonlinearities, the device dynamics essential to the network’s operation are accurately described by common linear approximations [29, 30], as discussed more below. In an I/O formulation, the tee is a 6-input and 6-output (6-I/O) itinerant field scattering device (three physical ports, each of which is both a field input and output, each field described by two quadrature degrees of freedom) with no internal degrees of freedom. The JPA is modeled as a 2-I/O, over-coupled linear resonator device (whose center frequency is a tunable parameter) with two internal degrees of freedom, representing the two quadratures of the mode inside the TKC [49, 50]. And the EMC is a 4-I/O device, with two I/O ports connected to a microwave field (effectively at zero temperature) and two I/O ports connected to a thermal mechanical bath. The EMC also con-

tains four internal degrees of freedom, representing the quadratures of coupled microwave and mechanical modes [10, 32, 33]. Fundamentally, when vacuum fluctuations in the microwave fields are significant, each instance of microwave dissipation inside each device or interconnection should be modeled using an additional I/O port pair [5] (and a beamsplitter component interrupting lossy interconnections), but such accuracy is not required below. It is well known that a network of linear, coherent I/O devices coupled to itinerant Gaussian fields may be modeled as a classical control system of interconnected, linear state space models [7–10]. The residual “quantumness” of these systems is captured by nonclassical “noise” driving the network inputs, but again, such quantum-level accuracy is not required below as the dynamics considered are classical. A linear network model representing the schematic depicted in Fig. 1b consists of ten coupled linear equations of motion, with six internal degrees of freedom, and two microwave and two mechanical bath I/O port pairs. Despite this complexity, standard control systems software toolkits make the construction of network dynamical models intuitive and efficient linear system theories may be applied to their analysis.

While the electromechanical interaction is fundamentally nonlinear, the dynamics we consider may be modeled by linearizing the coupling of the microwave and mechanical modes about a large microwave coherent state induced in the resonator by the coupling tone [29, 30], an approximation that is nearly ubiquitous in electromechanics. In a frame in which the EM degrees of freedom are rotating with the carrier frequency of the coupling tone, the Hamiltonian that describes the internal dynamics of the EMC in the linearized approximation is ($\hbar = 1$)

$$H_M = \Omega a_1^\dagger a_1 + \Delta a_2^\dagger a_2 + g(a_1 + a_1^\dagger)(a_2 + a_2^\dagger) \quad (1)$$

where a_1 is the annihilation operator for the mechanical mode and a_2 the annihilation operator for fluctuations in the microwave mode about the large coherent state ($a_{1,2}^\dagger$ the creation operators). Additionally, Ω is the center frequency of the oscillator, $\Delta = \omega_r - \omega_c$ is the frequency detuning between the resonator center frequency (ω_r) and coupling carrier (ω_c), and $g = g_0\sqrt{n_c}$, where n_c is the number of intra-resonator photons induced by the coupling tone.

In the usual I/O formulation for an EMC, the Heisenberg equations of motion may be represented in a rather condensed form by virtue of the fact that they describe a dynamical system that is both linear and fundamentally unitary [9, 10]. These restrictions on form ultimately stem from the need to preserve canonical commutation relations and are the primary distinction between coherent and more general linear I/O systems. For instance, we may write the I/O equations of motion for the EMC

as

$$\begin{aligned} \frac{d}{dt}\check{a} &= A_M \check{a} + B_M \check{b}_{in} \\ \check{b}_{out} &= C_M \check{a} + D_M \check{b}_{in} \end{aligned} \quad (2)$$

where $\check{a} = [a_1, a_2, a_1^\dagger, a_2^\dagger]^T$ (T indicating transpose), $\check{b}_{in} = [b_{Th,in}, b_{E,in}, b_{Th,in}^\dagger, b_{E,in}^\dagger]^T$, and similarly for \check{b}_{out} . Here, $b_{Th,in}$ and $b_{E,in}$ ($b_{Th,out}$ and $b_{E,out}$) are standard I/O theory objects that are functions of time t and may be roughly considered annihilation operators on the infinitesimal segment of free field incident on (leaving from) the device at time t [9]. Specifically, $b_{Th,in/out}$ and $b_{E,in/out}$ are associated with the fields that drive the system through the thermal mechanical port and the EMC's microwave port, respectively. As with a_2 , $b_{E,in/out}$ is associated with the microwave field fluctuations about the coupling tone amplitude. The matrices A_M , B_M , C_M , and D_M define the dynamics and despite their size are themselves represented by a relatively small number of variables. For instance, for general linear coherent systems in which the matrices C and D are block diagonal (i.e. no b_{out} is an explicit function of any b_{in}^\dagger or a^\dagger) these matrices may be broken down as [9]

$$\begin{aligned} A_M &= -\frac{1}{2}C_M^{*T}C_M + j\Pi_M, \quad B_M = -C_M^{*T}D_M, \\ C_M &= \text{diag}[\tilde{C}_M, \tilde{C}_M^*], \quad D_M = \text{diag}[\tilde{D}_M, \tilde{D}_M^*] \end{aligned} \quad (3)$$

where $*$ is the element-wise complex conjugation and j is the imaginary number with the electrical engineering sign convention [51]. The dynamics are thus completely defined by three matrices [32]

$$\begin{aligned} \tilde{D}_M &= \text{diag}[-1, -1], \quad \tilde{C}_M = \text{diag}[j\sqrt{\Gamma_0}, j\sqrt{\kappa_c}], \\ \Pi_M &= \begin{bmatrix} \Omega & g & 0 & g \\ g & \Delta + j\frac{\kappa_l}{2} & g & 0 \\ 0 & -g & -\Omega & -g \\ -g & 0 & -g & -\Delta + j\frac{\kappa_l}{2} \end{bmatrix} \end{aligned} \quad (4)$$

where Γ_0 is the intrinsic mechanical decay rate, κ_c (κ_l) is the EMC coupling (internal) decay rate. These expressions exemplify the high symmetry in all linear coherent I/O models. They may be reduced even further [9], but it doesn't suit our purposes to do so here.

Eqs. 2 are of a form equivalent to the state space representation of a linear system common in classical control theory. In a control context they would be succinctly referenced using an object \mathbb{M} that is defined by A_M , B_M , C_M and D_M and is often notated as [1, 9]

$$\mathbb{M} = \left[\begin{array}{c|c} A_M & B_M \\ \hline C_M & D_M \end{array} \right] \quad (5)$$

(each matrix and its location in the above array implies Eqs. 2). We can similarly generate state space model representations for the JPA and tee devices [9]; call them \mathbb{J} and \mathbb{T} , respectively.

We now come to the problem of constructing the network dynamical model. It has been previously pointed out that the formal equivalence between these quantum I/O models and the state space models that appear in classical linear control systems theory means that analogous procedures for constructing dynamical models in classical linear control systems also apply to linear quantum I/O ones [9]. Through these methods, we may derive a new state space model \mathbb{N} that describes the network as a whole. In the remainder of this section, it will be ambiguous whether we are constructing a quantum or coherent classical model. It is only when we neglect the effects of quantum fluctuation in the free fields when we compare our model to experiment that the approach becomes a classical approximation [11, 13].

The network model we need is depicted schematically in Fig. 2, as inspired by Fig. 1b, where the EMC and JPA each exchange input and output signals with two ports of the tee. The “ ψ ” and “ θ ” blocks represent the phase shifts accumulated just from transmission line delays around the tee-and-EMC and tee-and-JPA network loops, respectively (a more physical model would not lump these phase delays only on the input side of the tee, but half on each input and output. Up to unimportant phase shifts to the network internal variables, the two modeling approaches yield identical predictions). We thus define our network by defining the state space model objects \mathbb{T} , \mathbb{M} , and \mathbb{J} , and labeling the channels associated with each component's inputs and outputs according to the schematic Fig. 2. For instance the label “ E_o ” (the label “ E_o^* ”) in Fig. 2 is applied to both the

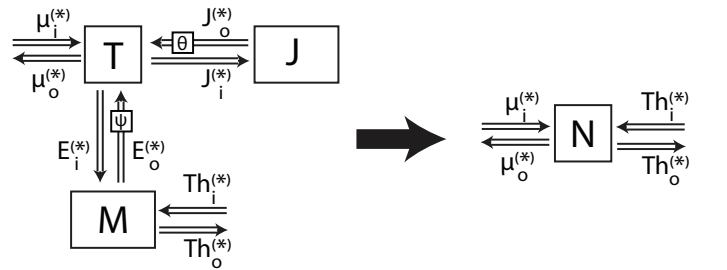


FIG. 2: Control system schematic of the network depicted in Fig. 1b. The tee, EMC and JPA components are represented as multi-input multi-output (MIMO) linear state space models that continually exchange signals. The interconnections are labeled here such that, e.g. $E_o^{(*)}$ stands for the two free field channels labeled E_o and E_o^* , which are explained in the text. Transmission line delays may be modeled here as static phase shifts ψ and θ . Standard software toolkits are available that reduce the network on the left to a single MIMO state space model \mathbb{N} . This approach is compatible with both quantum and classical investigations.

channel through which the \mathbb{M} output field represented by $b_{E,out}$ ($b_{E,out}^\dagger$) “flows” and the appropriate channel through which one of the \mathbb{T} inputs is driven. The label “ μ_i ” is applied only to the channel for the (heretofore unmentioned) $b_{\mu,in}$ field that drives the appropriate \mathbb{T} input representing one of the network’s microwave inputs, etc. While algorithmic, the construction of \mathbb{N} is extremely tedious. However, in the limit that transmission line delays may be accounted for by static, dispersionless phase shifts between the subcomponents, software toolboxes are available in, for example, Matlab and Mathematica that completely automate this model construction. This basic fact is under-recognized by the Physics community and deserves explicit emphasis: after defining the three state space models and labeling the component inputs and outputs according to Fig. 2, the entire state space model \mathbb{N} may be obtained in Matlab using the single command $\mathbb{N} = \text{connect}(\mathbb{T}, \mathbb{M}, \mathbb{J})$. (Other software that can deal with nonlinear quantum I/O networks has also been developed [13, 52]) Using such methods, these control systems toolkits determine an effective network state space model defined by matrices A_N (dimensions 6×6), B_N (6×4), C_N (4×6), and D_N (4×4),

$$\mathbb{N} = \left[\begin{array}{c|c} A_N & B_N \\ \hline C_N & D_N \end{array} \right], \quad (6)$$

which are too unwieldy to write out in general here.

It is useful, though, to consider the dynamical model for just a_2 , the annihilation operator for the microwave fluctuations in the EMC. For the EMC in isolation, and taking $g = 0$ for clarity, the equation of motion for this mode is

$$\frac{d}{dt} a_2 = \left(j\Delta - \frac{\kappa_t}{2} \right) a_2 - j\sqrt{\kappa_c} b_{E,in} \quad (7)$$

where $\kappa_t = \kappa_l + \kappa_c$. In the network \mathbb{N} , taking $g = 0$ and in the limit that the JPA has no internal loss and couples much more strongly to transmission lines than the EMC does, we find that

$$\frac{d}{dt} a_2 = \left(j\Delta'_{\theta'} - \frac{\kappa_n}{2} \right) a_2 + e^{-j(\lambda + \frac{1}{2}\psi)} \sqrt{\kappa'_c} b_{\mu,in} \quad (8)$$

where $\kappa_n = \kappa_l + \kappa'_c$ and

$$\begin{aligned} \kappa'_c &= \kappa_c \frac{\cos^2\left(\frac{\theta'}{2}\right)}{\cos^2\left(\frac{\theta'}{2}\right) \sin^2\left(\frac{\psi}{2}\right) + \cos^2\left(\frac{\psi + \theta'}{2}\right)} \\ \Delta'_{\theta'} &= \Delta - \kappa_c \frac{1}{4} \frac{\cos^2\left(\frac{\theta'}{2}\right) \sin(\psi) - \sin(\theta' + \psi)}{\cos^2\left(\frac{\theta'}{2}\right) \sin^2\left(\frac{\psi}{2}\right) + \cos^2\left(\frac{\psi + \theta'}{2}\right)} \\ \lambda &= \arctan\left(\cot\left(\frac{\psi}{2}\right) - \tan\left(\frac{\theta'}{2}\right)\right) \end{aligned} \quad (9)$$

where θ' is the total phase shift acquired by a narrow-

band signal that makes a round trip from the tee to JPA and back (i.e. is determined by the length of that interconnection and the center frequency of the JPA). Thus, in this approximation, the EMC resonator response still acts like a single-mode resonator, except one that is now driven by the inputs “ $\mu_i^{(*)}$ ” and has a new detuning from the carrier tone ($\Delta'_{\theta'}$), a new decay rate (κ_n), and a new phase shift between inputs and outputs (controlled by λ) that are all controlled by θ' , which is in turn controlled by the JPA center frequency. New effective system parameters, such as new effective decay rates and detunings, is a principle reason for constructing coherent feedback networks in general [6, 9, 10, 13]. In this case, these modifications quantitatively express the physical mechanisms qualitatively described in the last paragraph of the previous section. For example, the effective coupling rate κ'_c comes from the interference between signals emitted by \mathbb{M} that are passed to the network output directly and those that reflect off \mathbb{J} before being passed to the same output port. The effective detuning, $\Delta'_{\theta'}$, represents the interference between fields inside \mathbb{M} and those that exit \mathbb{M} , but are fed back into \mathbb{M} by the network. In general, and especially when intra-JPA loss is not negligible, these same qualitative effects still hold, although they lose their quantitative accuracy, in which case the full network model \mathbb{N} is needed.

If losses were negligible and the JPA bandwidth effectively infinite, the effective electrical parameters given in Eq. (9) could be substituted immediately into a traditional analysis of an electromechanical circuit [17, 19, 29, 30], whose physical interpretations are discussed in the previous section. Eq. (8) could also be extended to incorporate non-idealities with yet more complicated expressions, but this is beside the point. The modularity of the devices that make up the network permits us to use coherent network techniques to construct a dynamical model and make predictions using general and efficient algorithms. Analytic expressions of the full equations of motion are readily available, but they complicate matters unnecessarily here, and they are efficiently reproduced through the construction outlined above. Furthermore, we argue that such an approach is often efficient, useful, and appropriate as electromechanics and quantum engineering in general begins to move beyond the physics of individual devices.

In the next section, we compare the network model \mathbb{N} ’s steady state output predictions to data. This is most naturally done through a Laplace transform of the field and internal variables such that, e.g.

$$b_{\mu,in}[s] = \int_0^\infty e^{-st} b_{\mu,in} dt \quad (10)$$

where $b_{\mu,in}$ (as above) is a function of time. In the Laplace domain, it is appropriate to write the network equations of motion in terms of susceptibilities and trans-

fer functions such that [9]

$$\begin{aligned}\check{a}[s] &= (sI - A_N)^{-1} B_N \check{b}_{in}[s] \equiv \chi[s] \check{b}_{in}[s] \\ \check{b}_{out}[s] &= (C_N(sI - A_N)^{-1} B_N + D_N) \check{b}_{in}[s] \equiv \Xi[s] \check{b}_{in}[s]\end{aligned}\quad (11)$$

where $\check{a} = [a_1 a_2 a_3 a_1^\dagger a_2^\dagger a_3^\dagger]^T$ where a_3 is the annihilation operator on the internal JPA mode, $\check{b}_{in/out} = [b_{Th,in/out} b_{\mu,in/out} b_{Th,in/out}^\dagger b_{\mu,in/out}^\dagger]^T$, and I is an identity matrix of appropriate rank. While manually calculating the multi-input multi-output (MIMO) transfer function $\Xi[s]$ would be prohibitively tedious, again standard software toolboxes completely automate the procedure; in Matlab, given a network state space model N , the MIMO transfer function representation is obtained using the single command $\mathbf{Xi} = \mathbf{tf}(N)$.

The transfer function $\Xi[s]$ is applied several times in the next section to make predictions about the signals emitted by the network. For instance, the network's phase response to different frequency microwave probes is simulated in Fig. 4c by calculating the phase angle of the $\{\mu_o, \mu_i\}$ matrix element of $\Xi[s]$, angle $[\Xi_{\{\mu_o, \mu_i\}}[s]]$, as s runs along the imaginary axis. In general, the microwave-in-to-microwave-out response will be referred to as the network's S_{11} response. Similarly, the absolute value squared of the $\{\mu_o, Th_i\}$ matrix element of $\Xi[j\Omega]$, $|\Xi_{\{\mu_o, Th_i\}}[j\Omega]|^2$, represents the gain with which Ω -energy excitations in the thermal bath induce Ω -energy excitations in the microwave network output (i.e. induce blue sideband power in the network output), through effective $(b_{\mu_o, out}^\dagger b_{Th, in} + h.c.)$ -type interactions. Conversely, $|\Xi_{\{\mu_o^*, Th_i\}}[j\Omega]|^2$ represents the gain of thermal bath-induced Ω -energy de-excitations in the microwave network output (i.e. induction of red sideband power in the network output), through effective $(b_{\mu_o, out} b_{Th, in} + h.c.)$ -type interactions. The thermal-bath-in-to-microwave-out response will sometimes be referred to as the network's S_{12} response. Similarly,

$$\arg \max_{\delta\Omega} |\Xi_{\{\mu_o, Th_i\}}[j(\Omega + \delta\Omega)]|^2 \quad (12)$$

may be used to predict microwave-induced shifts in the mechanical center frequency [22, 44]. Finally, an expression related to $\chi[j\Omega]$, the $\{\mu_o, a_2\}$ matrix element of

$$C_N(j\Omega I - A_N)^{-1} jg \quad (13)$$

may be used to predict the rate with which oscillator excitations decay out the network blue sideband, potentially enhancing the total oscillator decay rate, and similar expressions may be used to predict red sideband decay and losses dissipated internally to the network. Thus, the functions $\Xi[s]$ and $\chi[s]$ are extremely convenient for modeling steady state network dynamics. And while the

matrix of expressions represented by $\Xi[s]$ is difficult for a human to parse, for instance, the object $\Xi[s]$ is easily manipulated algebraically and computationally.

RESULTS

The primary features of our network's operation are represented in Fig. 3. After this overview, various details are considered with greater depth. With the JPA far-detuned, the network's S_{11} phase response (i.e. the phase with which microwave tones are reflected by the network — see previous paragraph) near the center frequency of the EMC indicates an overcoupled, $\kappa_n/2\pi = 3$ MHz linewidth network resonance at 4.672 GHz, Fig. 3a. Driving with a strong coupling tone on this network resonance (and protecting the TKC with a cancellation tone), the thermal motion of the oscillator is visible via red and blue inelastically-scattered network output signals, i.e. sidebands. The power spectral densities of these sidebands (Fig. 3b) indicate a mechanical center frequency of $\Omega = 2\pi \times 713.6$ kHz and intrinsic damping rate of $\Gamma_0 = 2\pi \times 0.81$ Hz. By applying different amounts of external magnetic flux to the TKC, the apparent network resonance frequency and linewidth vary

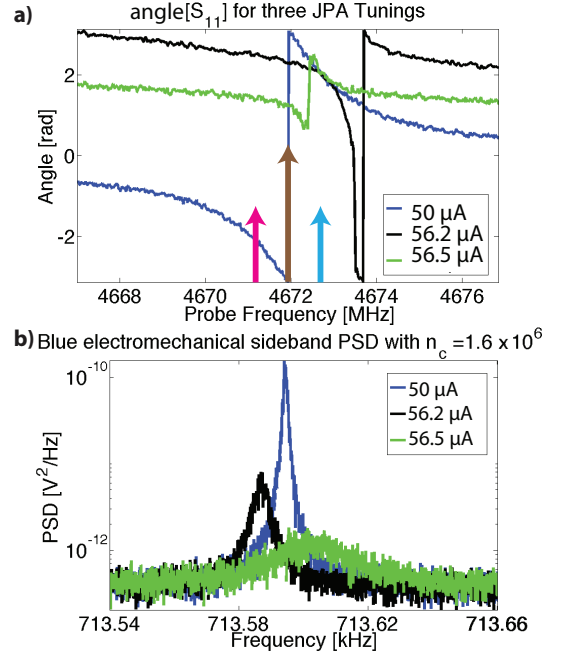


FIG. 3: a) Microwave probe measurements near the electromechanical network resonance for three flux bias settings. The JPA is far-detuned at 50 μA coil bias, but near-detuned for the others. The brown arrow represents an electromechanical coupling carrier tone on-resonant with the 50 μA -biased network. The blue and red arrows represent ± 714 kHz electromechanical sidebands. b) Employing $n_c = 1.6 \times 10^6$, the power spectral density of the blue sideband is shown for the three flux settings, keeping the coupling tone fixed.

together, each by values of order the EMC's coupling decay rate (Eqs. 9). As the network's response to probe tones varies, and with the strong coupling tone held at the same power and frequency, the characteristic mechanical motion inferred from the sidebands also varies. In particular, as the network's center frequency moves higher and its linewidth narrows, the apparent mechanical motion is damped more heavily (sideband linewidth becomes $\Gamma > \Gamma_0$), is cooled, and its center frequency moves ($\delta\Omega \neq 0$). These effects are analogous to sideband cooling in traditional electromechanical systems [17]. In our system, the origin of these effects may be interpreted as sideband cooling, or as the JPA acting as a coherent controller, exerting different control functions for different amounts of applied flux.

It is important to note that n_c , the number of photons in the EMC induced by the coupling tone, does not change as the TKC is tuned. While the network's electronic response to probes and mechanical sidebands varies with the TKC state, the coupling tone is canceled before the TKC and thus cannot be effected by it. More precisely, the mean power in the coupling tone is dissipated in the terminated port in the directional coupler through interference with the cancellation tone (Fig. 1a), while the information-carrying fluctuations about the mean coupling power are not. These fluctuations are thus fed back into the network after reflecting off the TKC and experience the effective network N (whose dynamics are approximated in Eq. (8)), while the coupling power experiences an entirely different network without TKC feedback (not discussed for sake of space). Except for inducing n_c , this coupling power is unimportant here and it carries no information. The assumption of a constant n_c is made throughout this section, and would have resulted in very inaccurate predictions in Figs. 5a and b (discussed below) if incorrect.

The network's response to microwaves may be finely tuned. Probing the network over a 2 GHz range, the JPA center frequency varies with applied flux, Fig. 4a. The other visible resonances, the narrow-band EMC and very broad-band resonances arising from standing waves between the subcomponents are only effected as the JPA tunes through them. Focusing on the 10 MHz band around the point the JPA tunes through the EMC ($\approx 56 \mu\text{A}$ flux coil bias; Fig. 4b), we see that as the flux increases, the network resonance first broadens slightly, then abruptly narrows and shifts higher, then becomes under-coupled, and finally re-broadens and returns to its original center. Device and network parameters may be precisely estimated given these 2 GHz and 10MHz probe ranges. In particular, we infer an EMC linewidth of $\kappa_c = 2\pi \times 2.7$ MHz and internal loss rate $\kappa_l = 2\pi \times .1$ MHz; a JPA linewidth of $\gamma = 2\pi \times 50$ MHz and internal loss rate of $\gamma_l = 2\pi \times 5$ MHz; and tee-to-EMC round trip phase shift of $\psi = 3.8$ rad and tee-to-JPA round trip phase shift of $\theta = 0.22$ rad. The tee

is assumed to be ideal and properly terminated, reflecting $1/9^{\text{th}}$ of the incident power with a 180° phase shift and splitting the remaining power between the other two ports. Although difficult to distinguish losses within the three over-coupled devices from interconnection losses, a loss model dominated by EMC and JPA internal losses is more consistent with observations than a model dominated by interconnection losses. Using these device parameters and a flux bias-to-JPA center frequency function, a linear control systems model built from interconnected device state space models using the Matlab Control Systems toolbox accurately reproduces the network's electronic response as the flux varies, Fig. 4c.

We now further consider the effects of this network on the oscillator dynamics. Driving the network at a frequency fixed near resonance when the JPA is far-detuned, $\Delta'_\theta = 2\pi \times 13$ kHz, and with a power such that $n_c = 1.6 \times 10^6$ is expected, we measure the linewidth and center frequency of the steady state mechanical sidebands emitted by the network as the flux is tuned, Figs. 5a & b. Starting from a linewidth of $\Gamma \approx \Gamma_0$ with the TKC far-detuned, Γ reaches a maximum of $2\pi \times 56$ Hz, with a simultaneous frequency shift of $\delta\Omega = -2\pi \times 24$ Hz, when the flux bias is $56.4 \mu\text{A}$. This flux bias corresponds to a JPA center frequency 3.4 MHz higher than the coupling tone, and an undercoupled network response with

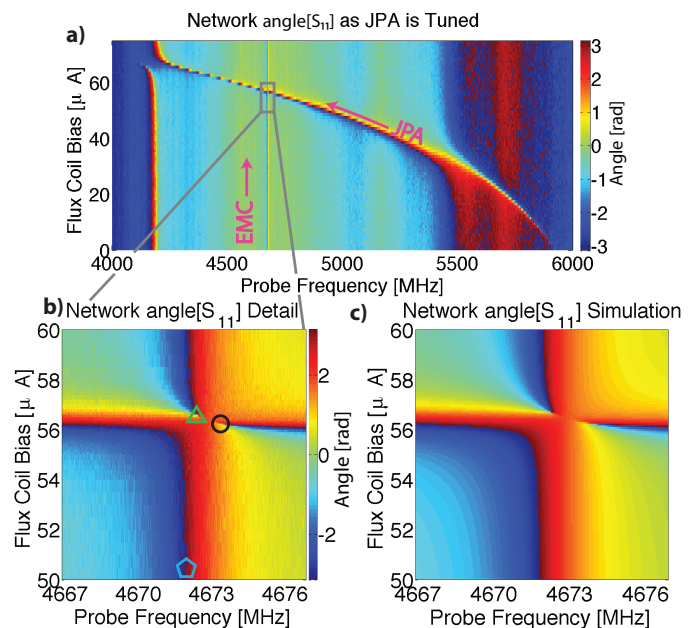


FIG. 4: a) Network's 4-6 GHz S_{11} phase response to microwave probes as flux bias is tuned. JPA resonance shifts with flux and couples to EMC (4.7 GHz) and standing wave (4.2 & 5.5 GHz) resonances as it passes through them. b) Detail of response around the EMC-JPA intersection. Points marked with pentagon, circle and triangle indicate network electromechanical center frequencies for the 50, 56.2 & 56.5 μA bias points depicted in Fig. 3. c) Simulation of response detail using a linear control systems model.

a ≈ 300 kHz internal loss rate. If losses in each network component had been lower, this effective internal loss rate would have been lower, and the maximum Γ on this plot could have been higher (note, for example, that the minimum κ_n of an ideal network is 0, see Eq. (9)). Because the $\Delta'_\theta \approx 0$ coupling tone has no significant effect on the mechanical state when the JPA is far-detuned, it is natural to interpret the JPA as “controlling” the oscillator as it is tuned through the EMC. Using a control-systems model (here employing standard-issue Mathematica toolkits) and no fit parameters, predictions for the expected mechanical linewidth and frequency shift as a function of flux bias are also included in Figs. 5a & b.

One metric for quantifying the efficiency with which the network controls the mechanics is the probability that a mechanically scattered photon dissipated by the network is a frequency up-converted photon minus the probability it is a down-converted photon. This “cooling efficiency” (CE) is independent of n_c , but is coupling-frequency dependent and is positive when the network cools the oscillator (and is negative when it amplifies

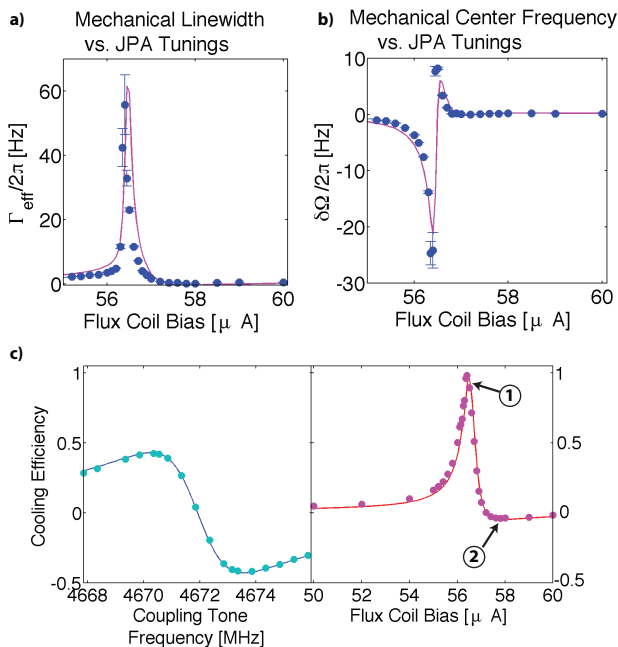


FIG. 5: a) Points represent the observed linewidth of blue thermal sidebands as the JPA is tuned, employing a $\Delta'_\theta = 2\pi \times 13$ kHz and $n_c = 1.6 \times 10^6$ coupling tone. The line is a theoretical prediction with no free parameters. b) From the same experiment, the observed changes in the oscillator center frequency and theoretical prediction are shown. c) Cooling efficiency (CE), as inferred from ring-down measurements and measured red and blue sideband powers. Left, CE for different coupling tone frequencies when JPA is far-detuned. Right, CE for $\Delta'_\theta = 2\pi \times 13$ kHz and different JPA tunings. Lines are theoretical predictions. Numbered call outs in right plot correspond to JPA tunings used in Fig. 6a.

thermal motion). The maximum CE obtainable over all coupling frequencies is $\Omega/\sqrt{\Omega^2 + \kappa_n^2}/4$, where κ_n is the total network EM linewidth. In Fig. 5c, left plot, we plot CE as a function of coupling tone frequency and with the JPA far-detuned. These are measured by first inducing coherent oscillations in the mechanics well above their thermal occupation through amplitude modulation of the coupling tone at frequency Ω , and then stopping the modulation and measuring the red and blue sidebands emitted by the network as the mechanical state re-equilibrates [53]. Data is averaged over 25 trials. The power emitted by both sidebands, P_{red} and P_{blue} , decays exponentially (“rings down”) in time at rate Γ , while $CE = (P_{blue} - P_{red}) / (P_{blue} + P_{red})$ is constant. The extremum of CE are ± 0.42 , implying a $\kappa_n/2\pi = 3$ MHz-linewidth network coupled to the significantly slower $\Omega/2\pi = 714$ kHz oscillator, an unresolved-sideband network. Underlying this data is the expected CE versus coupling frequency, using independent network and oscillator calibrations. Driving the network as in Figs. 5a&b and tuning the JPA, but now making ring down measurements, CE peaks at 0.98 at $56.4 \mu\text{A}$. A CE of 0.98 is only possible for networks with at most $\kappa_n/2\pi \approx 300$ kHz, a resolved-sideband network and a 10-fold reduction in κ_n consistent with the thermal data estimate above. Such a reduction was apparent from microwave S_{11} measurements in Figs. 4 & 3a, but CE represents an effective S_{12} measurement from the mechanical bath port to microwave output (i.e. S_{11} measurements test $\Xi_{\mu_o\mu_i}[s]$ while CE, S_{12} measurements test $\Xi_{\mu_oTh_i}[s]$). CE also reaches a minimum of -0.04 at $57.8 \mu\text{A}$, indicating that the network resonance can also dip slightly below its far-detuned JPA resonance. An independently calibrated control systems prediction using

$$CE = \frac{|\Xi_{\{\mu_oTh_i\}}[j\Omega]|^2 - |\Xi_{\{\mu_o^*Th_i\}}[j\Omega]|^2}{|\Xi_{\{\mu_oTh_i\}}[j\Omega]|^2 + |\Xi_{\{\mu_o^*Th_i\}}[j\Omega]|^2} \quad (14)$$

underlies the data.

Finally, we demonstrate that the state of the JPA, and thus the control it effects, may be switched far faster than the oscillator can equilibrate. While above we controlled the JPA state using static flux biasing, below we apply both static flux biasing and an additional, $\Delta'_\theta = 2\pi \times 10$ MHz microwave tone, whose amplitude is dynamically switched and is not cancelled at the directional coupler. At its strongest, this tone is too weak and off-resonant with the EMC to effect the oscillator, but is sufficiently strong and resonant with the wider-band TKC to strongly shift its center frequency. The rate with which the JPA may be switched in this manner should lie between the TKC linewidth (50 MHz) and the network’s EM linewidth as a whole (≥ 300 kHz), orders of magnitude faster than the mechanical response rate (0.81 Hz intrinsic linewidth). By performing similar ring down

measurements starting from an even larger mechanical coherent amplitude (inducing ~ 100 kHz pk-pk resonance shift in the EMC), this switched control may be observed with high visibility and bandwidth. In Fig. 6a, the power measured in the blue and red mechanical sidebands is depicted in time where, from 0 to 25 ms, the network is in a resolved-sideband and blue detuned state (state 1 in Fig. 6b, with CE called out in Fig. 5c), while from 25 to 40 ms, the network is in an unresolved-sideband and slightly red detuned state (state 2). In the first segment, almost all the mechanically-scattered power is in the blue sideband, and the total power emitted decays in time, indicating oscillator cooling (the large amplitude motion employed here induces a variation in the EMC center frequency of order the state 1 linewidth. As a consequence, the ring down power is more linear than exponential in time). In the second segment, the two powers are roughly equal, with the red sideband slightly greater, and the total power hardly decays. The inset depicts the transition between states 1 & 2, through which the blue sideband stays constant, but the red sideband power jumps by an order of magnitude. This is only possible because state 2 has a much larger linewidth than 1 (Fig. 6b). The

transition occurs at least as fast as the 25 kHz detection bandwidth, much faster than the mechanical decay rate in state 1 ($\Gamma_0 \ll \Gamma \sim 2\pi \times 15$ Hz) or 2 ($\Gamma_0 \gg \Gamma = 2\pi \times 0.1$ Hz).

Switched control over incoherent thermal motion may also be demonstrated, at the expense of reducing the detection bandwidth to 100 Hz (so that 10 min averaging times yield reasonable signal to noise ratios). In Fig. 6c and d, the coupling tone and JPA are tuned such that the mechanics are cooled for several seconds with $\Gamma = 2\pi \times 56$ Hz (the most aggressive, resolved-sideband cooling configuration in Fig. 5a). At time 100 ms, the JPA is rapidly far-detuned from the EMC, so that the network is on-resonance with the coupling tone and is in an unresolved sideband limit. For 500 ms, the mechanical state then thermalizes with its bath at rate Γ_0 . After 500 ms, the JPA is briefly tuned to the cooling state for 6 ms, and then back to the thermalization state for a final 400 ms. Fig. 6c depicts the 300-trial ensemble distribution of continuously monitored blue sideband amplitudes. Before 100 ms, the distribution is dominated by amplifier noise, but broadens by a factor of 3 during the thermalization periods. The sideband amplitude is proportional to mechanical position (by a factor that differs for the cooling and thermalization states), and the broadening of the distribution is indicative of a warming oscillator (to ~ 750 phonon occupation, or 26 mK, or $(63 \text{ Hz})^2$ variance in the EMC resonance, although precise knowledge of the thermal occupation is incidental to our purposes). The position variance of the hot $\Gamma = 2\pi \times 56$ Hz oscillator is expected to drop by e^{-2} in 6 ms, by e^{-1} in 3 ms, and the variance of the cold, Γ_0 -linewidth oscillator should rise to $1 - e^{-1}$ of the bath equilibrium value in 200 ms. Fig. 6d depicts the ensemble variance of 6 & 3 ms cooling-interval experiments and is consistent with these expectations.

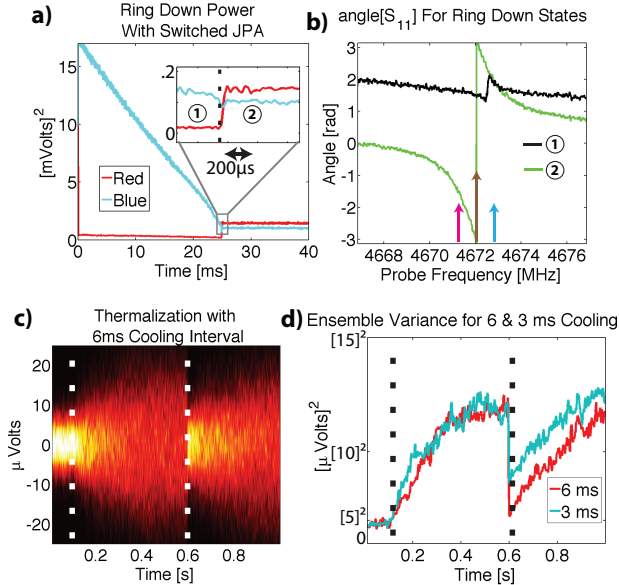


FIG. 6: Dynamic JPA-control. a) Red and blue sideband powers ringing down from a very high coherent amplitude. From 0-25 ms (25-40 ms) the network is in state 1 (state 2), see Figs. 5c & 6b. Inset, detail of network transition, depicted with 25 kHz bandwidth. b) Microwave probe S_{11} measurements for the network states employed in a, with arrows indicating coupling tone and sidebands. c) Switched rethermalization of a cooled oscillator. At 100 ms, JPA is tuned from $\Gamma \gg \Gamma_0$ (cooling) state to $\Gamma = \Gamma_0$ (bath-thermalizing) state. At 600 ms, JPA is switched to the cooling state for 6 ms only. Plot represents the ensemble distribution of blue sideband amplitudes in time for 300 trials. d) Sideband amplitude variance for 6 ms= $2/\Gamma$ and 3 ms= $1/\Gamma$ cooling-interval experiment ensembles.

CONCLUSION

We have demonstrated a small coherent feedback network of modular superconducting microwave devices that provides a degree of dynamically flexible control over a mechanical oscillator previously unavailable to the field of electromechanics. The network's operation has two natural interpretations: a dynamically-tunable input coupler [45, 46], or a gain-1 amplifier that receives and feeds coherent signals back to the oscillator and readout channel with a controlled phase shift [10]. Despite the simplicity of the components and construction (coaxial cabling between pre-existing and familiar superconducting devices), the network is too complex to be modeled using traditional electromechanical techniques (e.g., such approaches assume a single resonator mode, while our network features coupled resonators) [17, 29, 30]. However, it is efficiently and intuitively modeled using coherent network techniques [5, 7–10], an unconventional

approach that will find increasing utility as electromechanical research begins to move beyond the physics of individual devices. Although we only demonstrate this network's operation in the classical regime of mechanical motion and EM fields, on the basis of the well-known connections between classical and quantum dynamics in linear coherent systems [5, 7–11], we expect that the essential mechanisms of the network should work analogously in the presence of unambiguously quantum fields and states. We have not yet probed the quantum regime simply because of our use of a HEMT (non-quantum limited) amplifier for readout and the dynamical richness to be explored first in the classical regime.

There are several worthwhile directions for future investigations. First, the TKC may be pumped by a third microwave tone to add a parametric gain-and-squeezing element [28] (or a more general Kerr nonlinearity [13]) into the feedback and read-out dynamics. Recent theoretical work suggests that coherent feedback to an electromechanical system from a parametric gain controller can outperform any type of ideal measurement-based feedback or passive coherent controller [8, 10]. Second, the ability to dynamically and continuously modulate the network's coupling to its I/O port could be leveraged to shape the waveform of information-carrying signals read into and out of the EMC. This capability could facilitate high-fidelity coherent state transfer between the oscillator and arbitrary coherent devices either “up-” or “downstream” from the network [20, 46, 47]. And finally, the model could be considered from the perspective of well-developed theories of classical optimal and robust control [1, 7, 8, 10]. These sorts of investigations are likely to yield recommendations for a more precisely-controlled network construction. In particular, different applications are helped and hindered by different round trip phase shifts over the EMC and TKC network branches. While these phases were uncontrolled by the use of bulky cable interconnections in this work, a more integrated network could be constructed with much better precision.

We acknowledge partial support from the DARPA QuEST program, the DARPA ORCHID program, and from the NSF Physics Frontier Center at JILA. JK acknowledges the NRC for financial support.

* Electronic address: jkerc@jila.colorado.edu

- [1] K. J. Åström and R. M. Murray, *Feedback Systems: An Introduction for Scientists and Engineers* (Princeton University Press, Princeton, New Jersey, 2008).
- [2] H. M. Wiseman and G. J. Milburn, *Quantum Measurement and Control* (Cambridge University Press, Cambridge, England, 2009).
- [3] N. C. Jones *et al.*, Phys. Rev. X **2**, 031007 (2012).
- [4] H. Mabuchi, Appl. Phys. Lett. **98**, 193109 (2011).
- [5] J. Gough and M. R. James, IEEE Trans. Auto. Control. **54**, 2530-2544 (2009); Comm. in Math. Phys. **287**, 1109-1132 (2008).
- [6] J. Kerckhoff, H. I. Nurdin, D. S. Pavlichin, and H. Mabuchi, Phys. Rev. Lett. **105**, 040502 (2010).
- [7] M. R. James, N. I. Nurdin, and I. R. Petersen, IEEE Trans. Auto. Control. **53**, 1787 (2008).
- [8] H. I. Nurdin, M. R. James, and I. R. Petersen, Automatica **45**, 1847 (2009).
- [9] J. E. Gough, M. R. James, and H. I. Nurdin, Phys. Rev. A **81**, 023804 (2010).
- [10] R. Hamerly and H. Mabuchi, Phys. Rev. Lett. **109**, 173602 (2012).
- [11] H. Mabuchi, Phys. Rev. A **78**, 032323 (2008).
- [12] S. Iida, M. Yukawa, H. Yonezawa, N. Yamamoto, and A. Furusawa, IEEE Trans. Auto. Control. **57**, 2045 (2012).
- [13] J. Kerckhoff and K. W. Lehnert, Phys. Rev. Lett. **109**, 153602 (2012).
- [14] M. D. Reed, L. DiCarlo, S. E. Nigg, L. Sun, L. Frunzio, S. M. Girvin, and R. J. Schoelkopf, Nature (London) **482**, 382 (2012).
- [15] P. Schindler, J. T. Barreiro, T. Monz, V. Nebendahl, D. Nigg, M. Chwalla, M. Hennrich, and R. Blatt, Science **332**, 1059 (2011).
- [16] Z. Leghtas, G. Kirchmair, B. Vlastakis, R. Schoelkopf, M. Devoret, and M. Mirrahimi, arXiv:1207.0679.
- [17] T. J. Kippenberg and K. J. Vahala, Science **321**, 1172 (2008).
- [18] A. D. O’Connell *et al.*, Nature (London) **464**, 697 (2010).
- [19] J. D. Teufel, D. Li, M. S. Allman, K. Cicak, A. J. Sirois, J. D. Whittaker, and R. W. Simmonds, Nature (London) **471** 204, (2011).
- [20] T. A. Palomaki, J. W. Harlow, J. D. Teufel, R. W. Simmonds, and K. W. Lehnert, arXiv:1207.2944.
- [21] J. Chan *et al.*, Nature (London) **478**, 89 (2011).
- [22] J. D. Teufel, J. W. Harlow, C. A. Regal and K. W. Lehnert, Phys. Rev. Lett. **101**, 197203 (2008).
- [23] M. D. LaHaye, J. Suh, P. M. Echternach, K. C. Schwab, and M. L. Roukes, Nature **459**, 960 (2009).
- [24] J. B. Hertzberg, T. Rocheleau, T. Ndukum, M. Savva, A. A. Clerk, and K. C. Schwab, Nature Phys. **6**, 213 (2010).
- [25] F. Massel, S. U. Cho, J.-M. Pirkkalainen, P. J. Hakonen, T. T. Heikkilä, and M. A. Sillanpää, Nature Comm. **3**, 987 (2012).
- [26] C. A. Regal and K. W. Lehnert, Journal of Physics: Conference Series **264**, 1799 (2011).
- [27] R. W. Andrews *et al.*, *in preparation*.
- [28] M. A. Castellanos-Beltran, K. D. Irwin, G. C. Hilton, L. R. Vale, and K. W. Lehnert, Nature Phys. **4**, 929 (2008).
- [29] I. Wilson-Rae, N. Nooshi, W. Zwerger, and T. J. Kippenberg, Phys. Rev. Lett. **99**, 093901 (2007).
- [30] F. Marquardt, J. P. Chen, A. A. Clerk, and S. M. Girvin, Phys. Rev. Lett. **99**, 093902 (2007).
- [31] J. D. Teufel, T. Donner, M. A. Castellanos-Beltran, J. W. Harlow, and K. W. Lehnert, Nature Nanotechnol. **4**, 820 (2009).
- [32] T. Botter, D. W. C. Brooks, N. Brahms, S. Schreppler, and D. M. Stamper-Kurn, Phys. Rev. A **85**, 013812 (2012).
- [33] M. Tsang and C. M. Caves, Phys. Rev. Lett. **105**, 123601 (2010).
- [34] W. P. Smith, J. E. Reiner, L. A. Orozco, S. Kuhr, H. M. Wiseman, Phys. Rev. Lett. **89**, 133601 (2002).

- [35] M. A. Armen, J. K. Au, J. K. Stockton, A. C. Doherty, H. Mabuchi, Phys. Rev. Lett. **89**, 133602 (2002).
- [36] D. Kleckner and D. Bouwmeester, Nature **444**, 2 (2006).
- [37] T. Aoki *et al.*, Nat. Physics. **5**, 541-546 (2009).
- [38] C. Sayrin *et al.*, Nature (London) **477**, 73-77 (2011).
- [39] R. Vijay *et al.*, Nature (London) **490**, 77 (2012).
- [40] D. Ristè, C. C. Bultink, K. W. Lehnert, and L. DiCarlo, arXiv:1207.2944.
- [41] V. B. Braginsky, A. B. Manukin, and M. Y. Tikhonov, Sov. Phys. JETP **31**, 829 (1970).
- [42] S. Gigan *et al.*, Nature (London) **444**, 67 (2006).
- [43] O. Arcizet, P.-F. Cohadon, T. Briant, M. Pinard, and A. Heidmann, Nature **444**, 71 (2006).
- [44] K. R. Brown, J. Britton, R. J. Epstein, J. Chiaverini, D. Leibfried, and D. J. Wineland, Phys. Rev. Lett **99**, 137205 (2007).
- [45] M. D. Reed *et al.*, Appl. Phys. Lett. **96**, 203110 (2010).
- [46] Y. Yin *et al.*, arXiv:1208.2950.
- [47] J. I. Cirac, P. Zoller, H. J. Kimble, and H. Mabuchi, Phys. Rev. Lett., **78** 3221 (1997).
- [48] F. Diedrich, J. C. Bergquist, W. M. Itano, and D. J. Wineland, Phys. Rev. Lett. **62**, 403 (1989).
- [49] C. W. Gardiner and P. Zoller, *Quantum Noise* (Springer-Verlag, Berlin, 2004).
- [50] A. A. Clerk, M. H. Devoret, S. M. Girvin, F. Marquardt, and R. J. Schoelkopf, Rev. Mod. Phys. **82**, 1155 (2010).
- [51] While physicists tend to define a Fourier transform from the time to frequency domain as $f[w] = \int_{-\infty}^{\infty} f(t)e^{i\omega t} dt$ where i is the imaginary number, in electrical engineering contexts it is more common to find the same transform defined as $f[w] = \int_{-\infty}^{\infty} f(t)e^{-j\omega t} dt$ where j is the imaginary number.
- [52] N. Tezak, A. Niederberger, D. S. Pavlichin, G. Sarma, and H. Mabuchi, Phil. Trans. Roy. Soc. A **370**, 5270 (2012).
- [53] Besides representing a somewhat independent verification of the conclusions taken from the thermal data, these “ring down” measurements are more precise due to larger mechanical motion and motion that is phase-locked from trial to trial